Plasmonics (2025) 20:4149–4157
https://doi.org/10.1007/s11468-024-02530-y

RESEARCH

# High-Sensitivity D-Type Six-Hole PCF-SPR Sensor

Liying Xu[1] · Wei Liu[1] · Xingdi Luo[1] · Jingwei Lv[1] · Lin Yang[1] · Jianxin Wang[1] · Qiang Liu[1] · Paul K. Chu[2] · Chao Liu[1]

Received: 3 August 2024 / Accepted: 4 September 2024 / Published online: 29 October 2024


**Abstract**
Photonic crystal fiber (PCF) sensors based on surface plasmon resonance (SPR) have broad application prospects in biomedical sensing, food safety, chemical sensing, and other fields. However, many of the PCF-SPR sensors proposed so far have problems such as complicated structure, difficult fabrication, difficult fusion bonding with ordinary optical fibers, and low detection efficiency, which hinder the development of this technology. In order to reduce the difficulty of fiber fabrication, and improve the practicality of optical fiber, a D-type six-hole PCF-SPR sensor with a simple structure that can be fabricated easily is designed. In this structure, the cladding diameter is the same as that of the ordinary optical fiber, thus making it easier to fuse the two. By optimizing the structure of the sensor, the sensing characteristics are improved, as manifested by a maximum wavelength sensitivity and optimal resolution which are 36,000 nm/RIU and $2.78\times10^{-6}$RIU, respectively, in conjunction with a detectable refractive index range of 1.3–1.395. Because of these advantages, including a simple structure and high sensitivity, the sensor has great potential and value in many fields, such as biomedical sensing, chemical sensing, and so on.

**Keywords** Photonic crystal fiber · Surface plasmon resonance · High-sensitivity · Fabricated easily

## Introduction

Sensing technology is developing quickly and, together with communication technology and computer technology, constitutes the three pillars of the information industry. Surface plasmon resonance (SPR) photonic crystal fibers (PCFs) have great potential in sensing applications [1–5]. SPR is a physical optical phenomenon in which free electrons in a metal absorb the energy of incident light, and under specific conditions, electron oscillations occur. The SPR effect has a wide range of applications in bioscience, environmental monitoring and chemical research due to its high sensitivity, real-time and label-free monitoring [6]. PCF not only has all the advantages of conventional fiber, but also overcomes the problems of high transmission loss and narrow single-mode wavelength range of conventional fiber and has advantages in reducing fiber loss and achieving high non-linearity. The advantages of PCF are very significant, such as cut-off-free single mode transmission, good color dispersion, low bending loss, full-band transmission and high birefringence effect. The flexibility to change the geometrical shape, structural parameters and material properties of PCFs allows the optical properties to be varied to meet the needs of researchers, which is a great convenience for research work [7, 8]. PCF-SPR sensors are used in various fields, such as biomedical applications, as they can detect whether cells are cancerous by monitoring their refractive index, rendering them desirable in the prevention and treatment of diseases. In addition, PCF-SPR sensors are widely used in environmental protection, chemical sensing [9], food safety [10], and other fields.

The earliest SPR sensing devices were based on prisms, and although the performance of traditional prismatic SPR sensors is stable and reliable, a large number of mechanical components are required in the fabrication of the actual devices. Therefore, they are not suitable for real-time detection and sensing in practice due to the excessive size, high cost of fabrication, and difficulty in remote sensing [11]. SPR-based fiber optic sensors have gradually replaced

✉ Chao Liu
msm-liu@126.com

[1] School of Physics and Electronic Engineering, Northeast Petroleum University, Daqing 163318, People's Republic of China

[2] Department of Physics, Department of Materials Science and Engineering, Department of Biomedical Engineering, City University of Hong Kong, Tat Chee Avenue, Kowloon, Hong Kong, People's Republic of China

prism-based SPR sensors due to easy miniaturization, low fabrication cost, and real-time detection [12]. The properties of PCF-SPR sensors mainly depend on the plasmonic materials and PCF structure. Gold and silver are two common plasmonic materials due to their stable chemical properties [13], and the sensing properties can be further improved by optimizing the structural parameters of PCF-SPR sensors. In particular, D-type PCF sensors have garnered much interest.

Wu et al. have studied the sensing characteristics of side-polished PCF, which uses a wheel polishing device to side-polish the traditional PCF, and the polished D-type fiber not only reduces the refractive index of the Gaussian mode, which decreases the difficulty of phase matching, but also creates a flat surface on the fiber to facilitate the deposition of a metal film [14]. However, the metal film is prone to oxidization, resulting in unstable sensing [15, 16]. The unstable performance can be overcome by placing metal wires instead of using a traditional coating. W. Liu et al. have designed an ultra-sensitive hexagonal PCF-SPR sensor with a broad detection range, maximum wavelength sensitivity of 28,700 nm/RIU, and optimal resolution of $3.48\times10^{-6}$ RIU [17]. N. Islam et al. have proposed a sensitive open-channel-based PCF-SPR sensor for analyte refractive index sensing with a maximum wavelength sensitivity of 7000 nm/RIU and optimal resolution of $1.43\times10^{-5}$RIU [18]. Y. Fei et al. have proposed an efficient D-shape dual-core PCF-SPR sensor coated with an ITO Film for refractive index detection showing a maximum wavelength sensitivity of 22,100 nm/RIU [19]. However, most of these PCF-SPR sensors have a complex structure and are difficult to manufacture. In addition, because of the high cost of PCFs, PCFs are usually fused with common optical fibers in commercial applications. The cladding diameter of common optical fibers is usually 125 μm, but that of most PCFs is only a few tens of μm, thus leading to difficulty in fusion splicing between the PCFs and ordinary optical fibers. Therefore, it is important to reduce the difficulty in preparing optical fibers as well as fusion splicing between PCFs and common optical fibers [20].

In this work, a high-sensitivity D-type PCF-SPR sensor with a simple structure is designed and analyzed by the full-vector finite element method (FEM). There are only six rotationally and symmetrically distributed air holes in the cladding and the sensor can be prepared by polishing at any angle until one of the air holes is exposed for placement of a gold wire inside the air hole. The drawing technology for six-hole optical fibers is also mature making manufacturing straightforward. The diameter of the PCF is 125 μm, which is similar to that of common optical fibers, thereby reducing the difficulty of fusion splicing. Our results show that the sensor can detect a refractive index range from 1.3 to 1.395 with a maximum wavelength sensitivity of 36,000 nm/RIU, resolution of $2.78\times10^{-6}$RIU, and optimal quality factor of 119.87 $RIU^{-1}$. The sensor is not only simpler and easier to fabricate than most of the sensors that have been reported in terms of structural design, but also superior to most of the sensors in terms of performance. Besides, the sensor can be applied in biomedical, chemical sensing, food safety and other fields, which has a broad application prospect. For example, in the field of biomedicine, the sensor can be used to determine whether cells are cancerous or not by monitoring their refractive index. Table 1 shows the refractive indexes of common cells in the normal and cancerous states, which can be monitored by our PCF sensor [21].

## Model and Theory

In order to detect the change in the refractive index of the medium, a high-sensitivity sensor based on PCF-SPR is designed, as shown in Fig. 1. Figure 1a depicts the cross-section of the sensor, and Fig. 1b shows the three-dimensional view. The sensor contains six air holes with a diameter of $d$ and an air hole spacing of $\Lambda$. The simple sensor can be manufactured easily because the production of six-hole optical fibers is mature. In practical applications, photonic crystal fibers are often fused with ordinary optical fibers, and the cladding diameter of ordinary optical fibers is usually 125 μm. In order to reduce the fusion difficulty, the diameter of the cladding (blue area) of the sensor is set to 125 μm. To improve the sensing characteristics, the optical fiber is positioned sideway to shorten the distance between the analyte and the core, and a gold wire (gold area) is placed on the surface of the curved channel above the optical fiber to achieve coupling between the core fundamental mode and plasmonic mode. The diameter of the gold wire is $d_{Au}$, and the dielectric constant of gold can be derived by the Drude model [22]:

$$\varepsilon(\omega) = \varepsilon_{\infty} - \frac{\omega_p^2}{\omega\left(\omega + i\omega_c\right)}, \tag{1}$$

where $\varepsilon_{\infty}=9.75$ is the dielectric constant of gold in the high-frequency limit, $\omega_p=1.36\times10^{16}$ is the plasma frequency,

**Table 1** Refractive indexes of common cells in the normal and cancerous states

| Cancer types | Cell types | Refractive indexes of normal cells | Refractive indexes of cancerous cells |
|---|---|---|---|
| Skin | Basal | 1.360 | 1.380 |
| Cervical | Hela | 1.368 | 1.392 |
| Blood | Jurkat | 1.376 | 1.390 |
| Adrenal gland | PC12 | 1.381 | 1.395 |

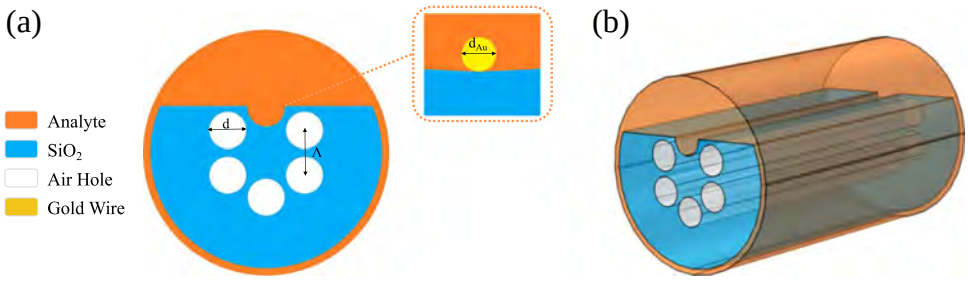


**Fig. 1** **a** Cross-section of the PCF-SPR sensor and **b** Three-dimensional view of the PCF-SPR sensor

$\omega_c = 1.45 \times 1014$ is the electron scattering frequency, and ω is the angular frequency of incident light.

The operation of the sensor is based on the SPR effect. With a light beam incident from the core to the cladding ($n_{core} > n_{cladding}$), it will generate a swift wave at the junction of the blue region and the orange region. Under the influence of the incident light, the free electrons on the surface of the gold wire generate collective oscillations, and the equipartitioned excitations generated by such collective oscillations are called the surface plasmonic wave. When the wave matches the surface plasmonic wave vector (effective refractive index of the real part of the core base mode and SPP mode are equal), the incident light wave transfers energy in the form of the surface plasmonic wave to create the SPR effect [23]. When the wave vectors of the passing wave and the surface plasmonic wave match (the effective refractive indexes of the core fundamental mode and the SPP mode are equal in real part), the incident light wave transfers the energy to the surface plasmonic wave to generate SPR.

The sensor is made of silicon dioxide, and its refractive index is determined by the Selmer's equation [24]:

$$n^2_{SiO_2}(\lambda) = 1 + \frac{A_1\lambda^2}{\lambda^2 - B_1} + \frac{A_2\lambda^2}{\lambda^2 - B_2} + \frac{A_3\lambda^2}{\lambda^2 - B_3}, \tag{2}$$

where $n$ is the refractive index of fused silica, $\lambda$ is the wavelength of the incident light, $A_1 = 0.696166300$, $A_2 = 0.407942600$, $A_3 = 0.897479400$, $B_1 = 4.67914826 \times 10^{-3}$ μm$^2$, $B_2 = 1.35120631 \times 10^{-2}$ μm$^2$, and $B_3 = 97.9340025$ μm$^2$.

Based on the principle of surface plasmon resonance, when the fundamental mode of the fiber core and the SPP mode satisfy phase matching, a part of the energy is transferred from the fundamental mode to the SPP mode, and the energy loss in the fiber core increases. The constraint loss (CL) in the fundamental mode is expressed as follows [25]:

$$\alpha_{loss}\left(\frac{dB}{cm}\right) = 8.686 \times \frac{2\pi}{\lambda} Im\left(n_{eff}\right) \times 10^4, \tag{3}$$

where $\lambda$ is the wavelength of the incident light and $Im(n_{eff})$ is the imaginary part of the effective refractive index of the optical fiber fundamental mode.

Figure 2 shows the dispersion curve versus the loss curve when the sensor undergoes surface plasmon resonance for an analyte refractive index of $n = 1.38$. With increasing incident light wavelength, the effective refractive indexes of the fundamental mode and SPP mode both decrease gradually in the real part and intersect at $\lambda = 1.6$ μm, meaning that the phase-matching condition is satisfied. When $\lambda < 1.6$ μm, the effective refractive index of the base mode of the core is lower than that of the SPP mode, and based on the SPR effect, the energy in the core is transferred to the metal surface, giving rise to an increase in the energy loss in the core. When $\lambda > 1.6$ μm, the effective refractive index of the fundamental mode is larger than that of the SPP mode, and the energy on the metal surface starts to be transferred back to the fiber core. Therefore, the energy loss in the fiber core decreases. Insets (a) and (b) show the electric field distributions of the core base mode and SPP mode, respectively, and inset (c) shows the electric field distributions of the core base mode and SPP mode when resonance coupling occurs. By comparing insets (a) and (c), it can be further verified that when the resonance condition is not reached, almost all the energy of the incident light is confined to the fiber core, whereas a part of the energy is transferred to the metal surface when the resonant coupling occurs.

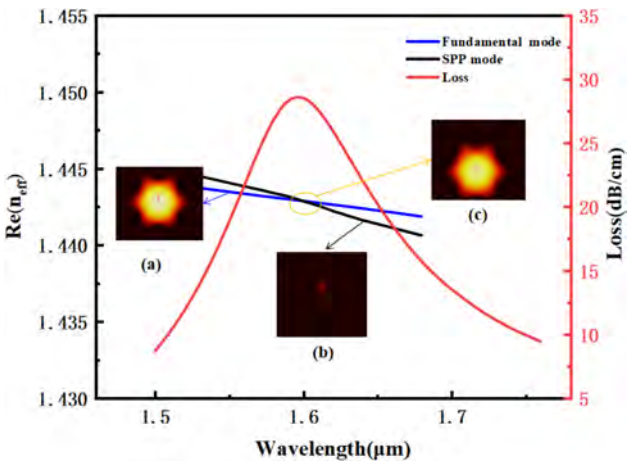


**Fig. 2** Loss curves of the base and SPP modes of the high-sensitivity SPR-PCF sensor for refractive index $n = 1.3$: **a** Fundamental mode, **b** SPP mode, and **c** SPR mode

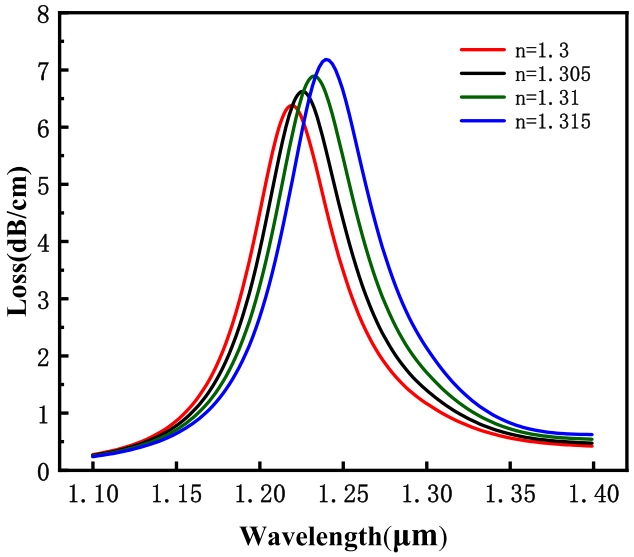


**Fig. 3** Loss curves for refractive indexes between 1.3 and 1.315

Figure 3 shows the loss spectra of the fiber core fundamental mode for refractive indexes between 1.3 and 1.315. As the refractive index changes, the loss curve of the fiber core fundamental mode shifts. The loss curve corresponding to each refractive index is unique, and the sensor is capable of high-precision sensing and detection of minute changes in the refractive index of the external medium.

The wavelength sensitivity, which is one of the important performance indicators of the sensor, can be derived by Eq. (4), which describes the variation of the resonance wavelength with refractive index [26]:

$$S_\lambda\left(\frac{nm}{RIU}\right) = \frac{\Delta\lambda_{peak}}{\Delta n_a}, \tag{4}$$

where $\lambda_{peak}$ is the resonance wavelength, and $\Delta n_a$ is the difference in the refractive index change of the analyte.

The resolution is another important parameter in a sensor reflecting the smallest change the sensor can distinguish. The resolution is expressed as follows [27]:

$$R(RIU) = \Delta n_a \times \frac{\Delta\lambda_{min}}{\Delta\lambda_{peak}}, \tag{5}$$

where $\Delta\lambda_{min}$ is the minimum spectral resolution, generally taken as 0.1 nm, $\Delta n_a$ is the difference in refractive indices, and $\lambda_{peak}$ is the displacement between the two resonant wavelengths.

In addition, the quality factor or figure of merit (FOM) dictates the performance. The FOM is the ratio of the wavelength sensitivity to the full-width at high-maximum (FWHM). Usually, the larger the FOM, the higher the detection accuracy. The FOM can be expressed as [28]:

$$FOM = \frac{s_\lambda}{FWHM}, \tag{6}$$

where $S_\lambda$ is the wavelength sensitivity and FWHM is the full-width at half-maximum of the peak loss in nm.

## Optimization of Sensor Parameters

In order to improve the detection capability of the PCF-SPR sensor, the gold wire diameter $d_{Au}$, air hole spacing $\Lambda$, air hole diameter $d$, and polishing depth $L$ are optimized based on the wavelength sensitivity and FOM as the optimization criteria. The initial parameters are $d_{Au}=0.6$ μm, $\Lambda=25$ μm, $d=20$ μm, and $L=37.5$ μm.

Figure 4 shows the effects of the gold wire diameter $d_{Au}$ on the loss spectra of the fundamental mode of the PCF-SPR sensor. When the gold wire diameter $d_{Au}$ increases from 0.4

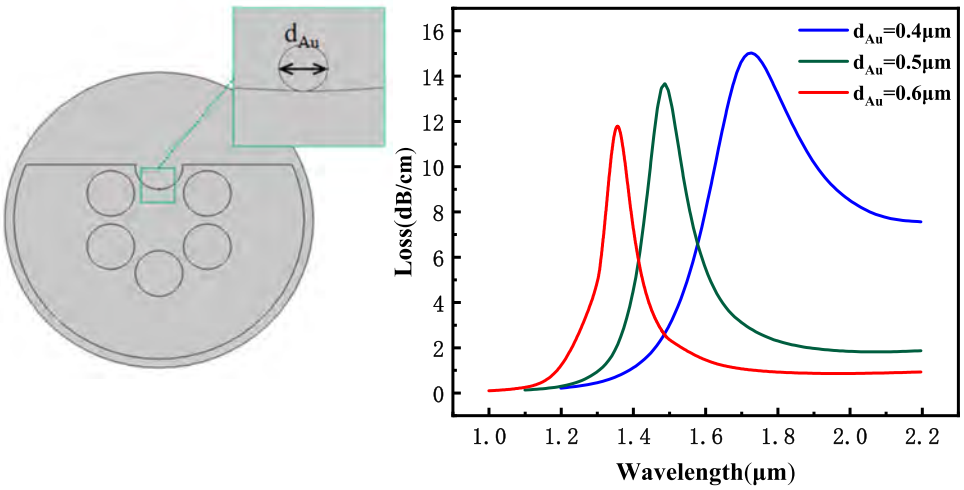


**Fig. 4** Effects of different gold wire diameters $d_{Au}$ on the loss spectra of the PCF-SPR sensor

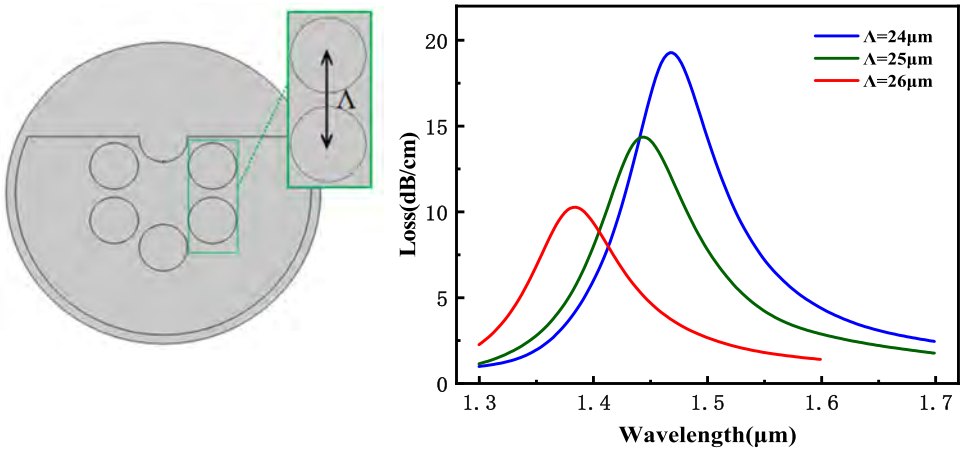


**Fig. 5** Effects of the air hole spacing $\Lambda$ on the loss spectra of the PCF-SPR sensor

to 0.6 μm, the loss curves blueshift. That is, the resonance wavelength shifts in the direction of a shorter wavelength. This is because as the diameter of the gold wire increases, the wave that can penetrate the gold wire decreases, and more energy is confined to the fiber core, consequently improving the refractive index of the fundamental mode, reducing the phase velocity of the incident light wave, and shortening the resonance wavelength. Figure 4 shows that when the diameter of the gold wire is 0.6 μm, the loss curve is the sharpest, i.e., the smallest FWHM, indicating that the detection accuracy is the best. Therefore, the diameter of the gold wire, $d_{Au}$, is set to 0.6 μm.

Figure 5 shows the effects of the air hole spacing $\Lambda$ on the loss spectra of the PCF-SPR sensor. When the air hole spacing $\Lambda$ increases from 24 to 26 μm with an increment of 0.1 μm, the resonance wavelength blueshifts because as the air hole spacing becomes larger, more energy is bound to the fiber core. The refractive index of the fiber core is larger, and the phase velocity of the incident wave becomes slower. The resonance wavelength becomes shorter, and the loss peak gradually becomes smaller in this process, indicating that the coupling effect between the fundamental mode of the fiber core and the SPP mode worsens. Therefore, the air hole spacing $\Lambda$ is set to 24 μm.

Figure 6 shows the effects of the air hole diameter $d$ on the loss spectra of the PCF-SPR sensor. When the air hole diameter $d$ increases from 19.6 to 20.4 μm with an increment of 0.4 μm, the resonance wavelength redshifts because with increasing air hole diameter, the duty cycle increases. The refractive index of the fiber core becomes smaller, and the energy bound to the fiber core decreases. The phase velocity of the incident light in the fiber core is higher, the resonance wavelength becomes larger, and the loss peak gradually increases, indicating that the fiber core fundamental mode is coupled with the SPP mode more effectively. According to Eq. (4), the wavelength sensitivity is calculated to be 500 nm/RIU for air hole diameters of 19.6 μm and 20 μm, and 600 nm/RIU for an air hole diameter of 20.4 μm. The optimal air hole diameter $d$ is thus 20.4 μm.

A critical parameter of the D-shape fiber is the grinding depth represented by $L$ in this structure. Figure 7 shows the effects of the grinding depth $L$ on the loss spectra of the SPR sensor. When $L$ increases from 37.5 to 38.5 μm with an increment of 0.5 μm, the refractive index of the cladding

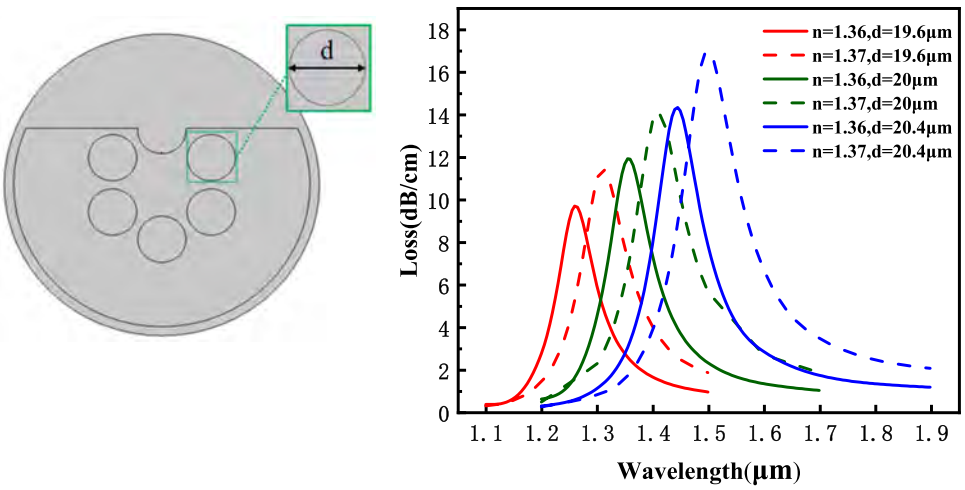


**Fig. 6** Effects of the air hole diameter $d$ on the loss spectra of the PCF-SPR sensor

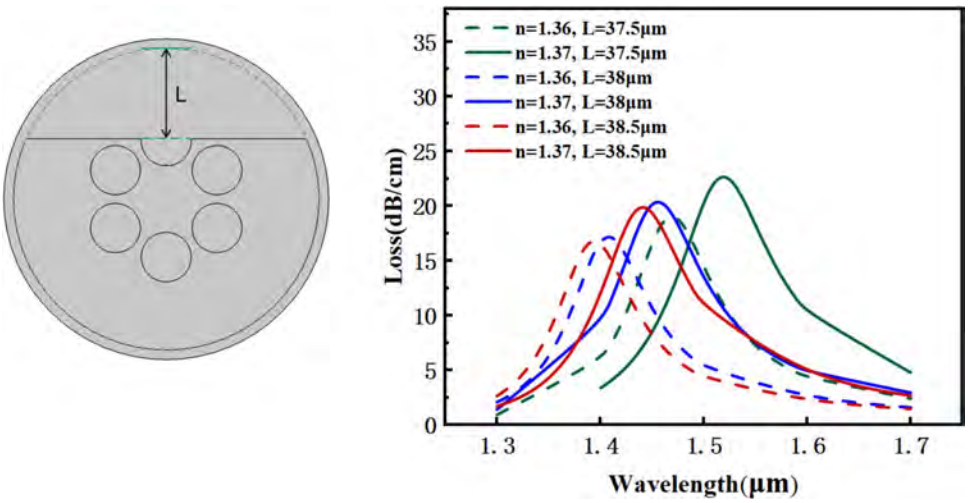


**Fig. 7** Effects of the polishing depth $L$ on the loss spectra of the PCF-SPR sensor

decreases. The refractive index of the core becomes relatively large, the energy constrained to the core increases, the phase velocity of the incident light decreases, and the resonance wavelength blueshifts. According to Eq. (4), the effects of the grinding depth on the wavelength sensitivity are almost constant. In actual polishing, the deeper the polishing depth of the optical fiber, the easier the optical fiber breaks. Hence, the optical fiber polishing depth $L$ is set to 37.5 μm.

Figure 8a shows the loss spectra of the base mode of the fiber core when the refractive index of the analyte is changed from 1.3 to 1.395. As the refractive index of the analyte increases, the peak of the loss curve increases, indicating that most of the energy in the fiber core is transferred to the metal surface, resulting in a decrease in the refractive index of the fiber core, an increase in the phase velocity of the incident light wave, and a red-shift in the loss curve. The PCF-SPR sensor can detect analytes with refractive indexes between 1.3 and 1.395. Figure 8b shows the polynomial fit of the resonance wavelength with an R-square of 0.99.

In conclusion, by optimizing the gold wire diameter $d_{Au}$, air space distance $\Lambda$, air diameter $d$, and polishing depth $L$, the maximum wavelength sensitivity of the sensor increases from 34,000 to 36,000 nm/RIU.

## Characteristics of the PCF-SPR Refractive Index Sensor

In order to better evaluate the sensor performance, the wavelength sensitivity (S)λ, resolution (R), and figure of merit (FOM) are studied. Figure 9a shows the wavelength sensitivity for different refractive indexes. The wavelength sensitivity increases from 1200 to 36,000 nm/RIU when the refractive index increases from 1.3 to 1.395. Figure 9b shows the FWHM and FOM for different refractive

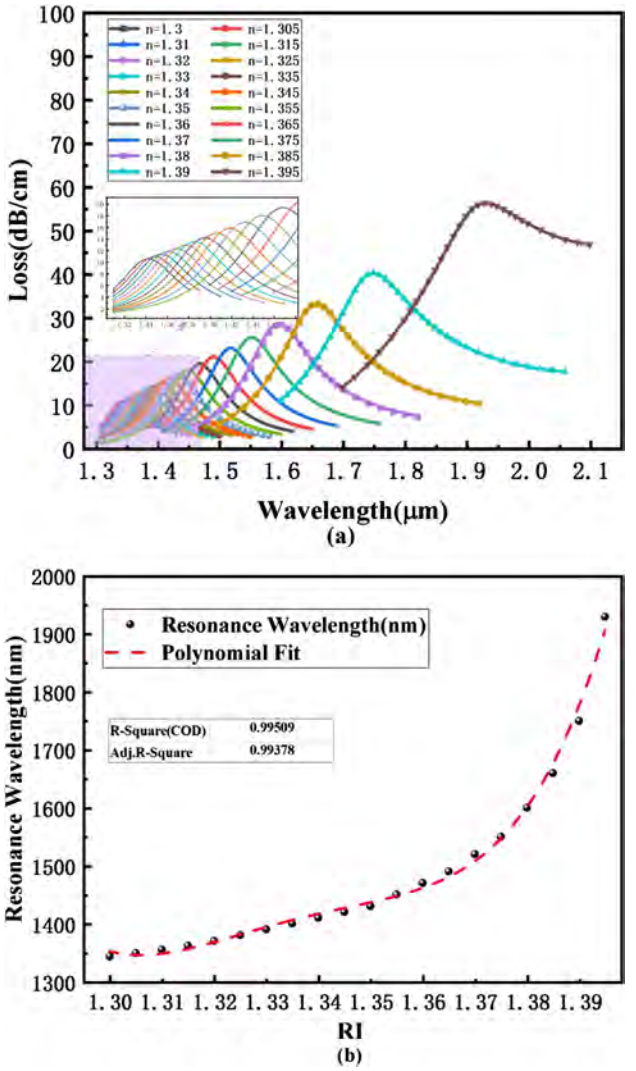


**Fig. 8** **a** Loss spectra in the RI range of 1.29–1.39 and **b** polynomial fit of the resonance wavelengths

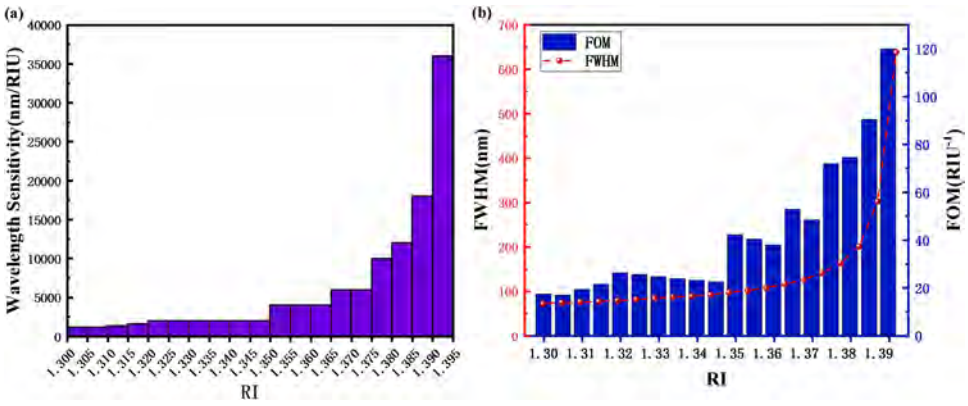


**Fig. 9** **a** Wavelength sensitivity and **b** full-width at half-maximum (FWHM) and figures of merit (FOM)

indexes, revealing an increasing trend for both, with the best FOM being 119.87 $RIU^{-1}$. Table 2 shows the wavelength sensitivity and resolution of the sensor, suggesting large application potential.

As shown in Table 2, in the RI range of 1.3–1.395, the wavelength sensitivity of the PCF-SPR sensor increases from 1200 to 36,000 nm/RIU, with the maximum being 36,000 nm/RIU, corresponding to a resolution of $2.78 \times 10^{-6}$ RIU and the best quality factor of 119.87 $RIU^{-1}$. The resolution of the SPR sensor increases, meaning that it is possible to detect tiny changes to boost the sensitivity.

**Table 2** Sensing characteristics of the PCF-SPR sensor

| Analyte RIs | WS (nm/RIU) | R(RIU) | FWHM (nm) | FOM($RIU^{-1}$) |
|---|---|---|---|---|
| 1.3 | 1200 | $8.33\times10^{-5}$ | 70.31 | 17.07 |
| 1.305 | 1200 | $8.33\times10^{-5}$ | 72.17 | 16.63 |
| 1.31 | 1400 | $7.14\times10^{-5}$ | 73.48 | 19.05 |
| 1.315 | 1600 | $6.25\times10^{-5}$ | 75.16 | 21.29 |
| 1.32 | 2000 | $5\times10^{-5}$ | 76.89 | 26.01 |
| 1.325 | 2000 | $5\times10^{-5}$ | 79.08 | 25.29 |
| 1.33 | 2000 | $5\times10^{-5}$ | 81.90 | 24.42 |
| 1.335 | 2000 | $5\times10^{-5}$ | 84.80 | 23.58 |
| 1.34 | 2000 | $5\times10^{-5}$ | 87.52 | 22.85 |
| 1.345 | 2000 | $5\times10^{-5}$ | 90.30 | 22.15 |
| 1.35 | 4000 | $2.5\times10^{-5}$ | 95.30 | 41.97 |
| 1.355 | 4000 | $2.5\times10^{-5}$ | 99.88 | 40.05 |
| 1.36 | 4000 | $2.5\times10^{-5}$ | 106.03 | 37.73 |
| 1.365 | 6000 | $1.67\times10^{-5}$ | 114.04 | 52.61 |
| 1.37 | 6000 | $1.67\times10^{-5}$ | 124.43 | 48.22 |
| 1.375 | 10,000 | $1\times10^{-5}$ | 139.35 | 71.76 |
| 1.38 | 12,000 | $8.33\times10^{-6}$ | 161.28 | 74.41 |
| 1.385 | 18,000 | $5.56\times10^{-6}$ | 199.33 | 90.30 |
| 1.39 | 36,000 | $2.78\times10^{-6}$ | 300.34 | 119.87 |
| 1.395 | N/A | N/A | 637.51 | N/A |

## Discussion

In the manufacturing process, the preparation of six-hole optical fibers is mature. The existing technology can easily fabricate six-hole optical fibers and side-polish the six-hole photonic crystal optical fibers. After polishing, precision tools such as microscopes and mechanical arms are used to hold one end of the gold wire. The gold wire can be formed steadily on the surface of the curved channel to adjust to the nearest position to the core. Finally, laser welding or curing adhesive is applied to fix the gold wire on the optical fiber.

The optimized sensor can detect analytes with refractive indexes ranging from 1.3 to 1.395, as shown in Fig. 10. SMF is used to fuse the two sides of the PCF-SPR sensor, one end being connected to a broadband light source and the other end to a spectrum analyzer (OSA). The sensor is fixed on the slide and then placed on the carrier table. The analyte is added to the slide to make full contact with the sensor. When light passes through the SMF and enters the SPR-SPR sensor, a part of it is transferred from the fiber core to the metal surface, where it undergoes plasmonic excitations on the metal surface to excite the SPR. As the refractive index of the analyte varies, the SPR resonance peak shifts, and the change is monitored by the OSA and computer.

To highlight the advantages of the PCF-SPR sensor, Table 3 compares the characteristics of different sensors. Our sensor has the biggest detectable refractive index range and the largest maximum wavelength sensitivity. More importantly, as aforementioned, the sensor is easy and economical to manufacture.

## Conclusion

A PCF-SPR refractive index sensor is designed and its coupling characteristics and sensing properties are analyzed numerically by the finite element method. The sensitivity of the PCF-SPR sensor can be improved by optimizing the structural parameters. The results show that

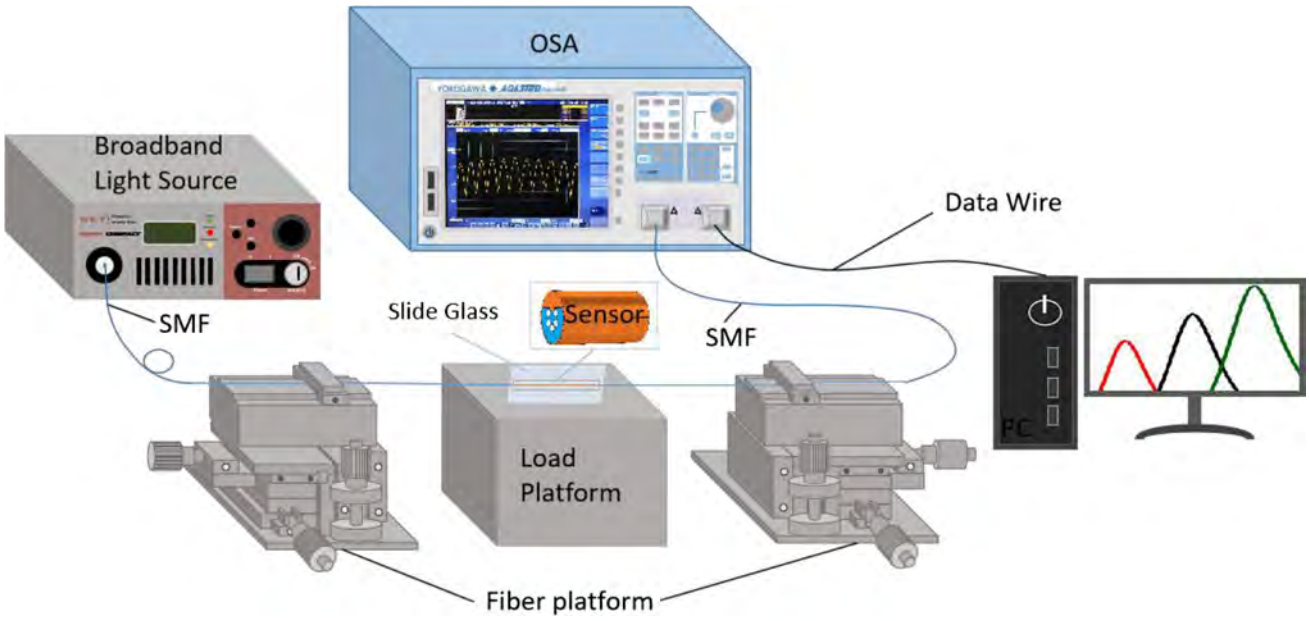


**Fig. 10** Schematic diagram of the setup for refractive index detection

**Table 3** Comparison of the characteristics between our PCF-SPR sensor and similar PCF-SPR sensors reported recently

| Refs. | Detection range | WS (nm/RIU) | R(RIU) | Structure diagram |
|---|---|---|---|---|
| [18] | 1.33–1.4 | 7000 | $1.43\times10^{-5}$ | |
| [29] | 1.33–1.42 | 11,000 | $7\times10^{-6}$ | |
| [30] | 1.35–1.41 | 20,000 | $5\times10^{-6}$ | |
| [31] | 1.33–1.365 | 13,600 | $7.35\times10^{-6}$ | |
| Proposed | 1.3–1.395 | 36,000 | $2.78\times10^{-6}$ | |

the sensor is capable of detecting a refractive index range between 1.3 and 1.395 with a maximum wavelength sensitivity of 36,000 nm/RIU and resolution of $2.78\times10^{-6}$ RIU. It can be used to monitor and analyze molecules, cells, and tissues in biological samples. By measuring the changes in the refractive index of the analyte, the sample composition, concentration, and quality can be determined. For example, the changes in the refractive index of cells such as Basal, Hela, Jurkat, PC12, etc. can be monitored to determine whether they are cancerous. The PCF-SPR sensor, with a simple structure, excellent sensing characteristics, and remarkable utility, has immense potential in applications in the biomedical field.

**Author Contributions** Liying Xu: Conceptualization, Methodology, Software, Writing-Original Draft. Wei Liu: Investigation, Validation. Xingdi Luo: Conceptualization, Writing- Reviewing and Editing. Jingwei Lv: Formal analysis. Lin Yang: Funding acquisition, Validation. Jianxin Wang: Investigation.,Conceptualization. Qiang Liu: Resources. Paul K. Chu: Project administration. Chao Liu: Resources, Writing-Reviewing and Editing.

**Funding** This work was jointly supported by the Heilongjiang Provincial Natural Science Foundation of China [JQ2023F001], National Natural Science Foundation of China [12304480], Local Universities Reformation and Development Personnel Training Supporting Project from Central Authorities, Natural Science Foundation of Heilongjiang Province [LH2021F007], China Postdoctoral Science Foundation funded project [2020M670881], as well as City University of Hong Kong Donation Research Grants [DON-RMG 9229021 and 9220061], Outstanding young and middle-aged research and innovation team of Northeast Petroleum University [KYCXTD201801].

**Data Availability** Data underlying the results presented in this paper are not publicly available at this time but may be obtained from the authors upon reasonable request.

## Declarations

**Conflict of Interest** The authors declare no competing interests.

## References


1. Liu W, Shi Y, Yi Z et al (2021) Surface plasmon resonance chemical sensor composed of a microstructured optical fiber for the detection of an ultra-wide refractive index range and gas-liquid pollutants[J]. Opt Express 29(25):40734–40747
2. Fu HY, Zhang SW, Chen H, Weng J (2015) Graphene enhances the sensitivity of fiber-optic surface plasmon resonance biosensor. IEEE Sensors J 15(10):5478–5482
3. Liu W, Liu C, Wang J et al (2023) Surface plasmon resonance sensor composed of microstructured optical fibers for monitoring of external and internal environments in biological and environmental sensing[J]. Results in Physics 47:106365
4. Ng WL, Rifat AA, Wong WR, Mahdiraji GA, Adikan FM (2018) A novel diamond ring fiber-based surface plasmon resonance sensor. Plasmonics 13(4):1165–1170
5. Lou JB, Cheng TL, Li SG (2019) High sensitivity photonic crystal fiber sensor based on dual-core coupling with circular lattice. Opt Fiber Technol 48:110–116
6. Khurana K, Jaggi N (2021) Localized surface plasmonic properties of Au and Ag nanoparticles for sensors: a review[J]. Plasmonics 16(4):981–999
7. Kubota H, Kawanishi S, Koyanagi S et al (2004) Absolutely single polarization photonic crystal fiber[J]. IEEE Photonics Technol Lett 16(1):182–184
8. Tawfiq ZH, Fakhri MA, Adnan SA (2018) Photonic crystal fibres PCF for different sensors in review[C]//IOP conference series: materials science and engineering. IOP Publishing 454(1):012173
9. Zhao Z, Zhang A, Pan H et al (2024) Wide detection range and sensitivity enhanced dual eccentric-core d-shaped photonic crystal fiber surface plasmon resonance sensor[J]. Plasmonics 19(3):1659–1666
10. Liu C, Yang L, Liu Q, Wang FM, Sun ZJ, Sun T et al (2018) Analysis of a surface plasmon resonance probe based on photonic crystal fibers for low refractive index detection. Plasmonics 13(3):779–784
11. Klantsataya E, Jia P, Ebendorff-Heidepriem H et al (2017) Plasmonic fiber optic refractometric sensors: from conventional architectures to recent design trends[J]. Sensors 17(1):12
12. Liu Q, Hou S, Lei J (2022) Design and analysis of d-shaped surface plasmon resonance fiber biosensor for liquid analytes[J].
13. Tian Y, Zhang L, Wang L (2020) DNA-functionalized plasmonic nanomaterials for optical biosensing[J]. Biotechnol J 15(1):1800741
14. Wu T, Shao Y, Wang Y et al (2017) Surface plasmon resonance biosensor based on gold-coated side-polished hexagonal structure photonic crystal fiber[J]. Opt Express 25(17):20313–20322
15. Liu Q et al (2020) The biochemical sensor based on liquid-core photonic crystal fiber filled with gold, silver and aluminum. Opt Laser Technol 130:106363
16. Hasan MR et al (2018) Plasmonic refractive index sensor employing niobium nanofilm on photonic crystal fiber. IEEE Photonics Technol Lett 30(4):315–318
17. Liu W, Hu C, Zhou L et al (2020) Ultra-sensitive hexagonal PCF-SPR sensor with a broad detection range[J]. J Mod Opt 67(20):1545–1554
18. Islam N, Arif MFH, Yousuf MA et al (2023) Highly sensitive open channel based PCF-SPR sensor for analyte refractive index sensing[J]. Results in Physics 46:106266
19. Fei Y, Luo B, An M et al (2024) A highly efficient d-shaped dual-core PCF-SPR sensor coated with ITO film for refractive index detection[J]. Plasmonics 1–15
20. Wu C, Song N, Cao C et al (2019) Bending characteristic analysis and improvement of fusion splice between photonic crystal fiber and single mode fiber[J]. Optics Communications 435:190–194
21. Jabin MA, Ahmed K, Rana MJ, Paul BK, Islam M, Vigneswaran D, Uddin MS (2019) Surface plasmon resonance based titanium coated biosensor for cancer cell detection. IEEE Photonics J 11(4):1–10
22. Bing PB, Liu Q, Wu GF, Yuan S, Li ZY, Du HL et al (2022) A plasmonic sensor based on D-shaped dual-core microchannel photonic crystal fiber. Plasmonics 17(4):1471–1478
23. Kadhim RA, Yuan L, Xu H et al (2020) Highly sensitive D-shaped optical fiber surface plasmon resonance refractive index sensor based on Ag-α-$Fe_2O_3$ grating. IEEE Sens J 20(17):9816–9824
24. Liu C, Wang J, Wang F et al (2020) Surface plasmon resonance (SPR) infrared sensor based on d-shape photonic crystal fibers with ITO coatings[J]. Opt Commun 464:125496
25. Hu L, Li J, Li S et al (2024) A dual-core two-parameter of RI and temperature photonic crystal fiber sensor based on the SPR effect[J]. Plasmonics 19(3):1667–1678
26. Zhou C (2013) Theoretical analysis of double-microfluidic-channels photonic crystal fiber sensor based on silver nanowires. Opt Commun 288:42–46
27. Meshginqalam B, Barvestani J (2021) Comparative study of the highly sensitive plasmonic sensor based on a D-Shaped photonic crystal fiber with silver or gold layers. Physica Scr 96(12):125535
28. Gandhi MA, Chu S, Senthilnathan K, Babu PR, Nakkeeran K, Li Q (2019) Recent advances in plasmonic sensor-based fiber optic probes for biological applications. Appl Sci 9(5):949
29. Rifat AA, Haider F, Ahmed R et al (2018) Highly sensitive selectively coated photonic crystal fiber-based plasmonic sensor[J]. Opt Lett 43(4):891–894
30. Jiang H, Shen T, Feng Y et al (2023) Characterization of incompletely coated D-shaped PCF-SPR refractive index sensors[J]. Phys Scr 98(10):105520
31. Jiao S, Gu S, Yang H et al (2018) Highly sensitive dual-core photonic crystal fiber based on a surface plasmon resonance sensor with a silver nano-continuous grating[J]. Appl Opt 57(28):8350–8358